

ARTICLE OPEN



Ultra-high field imaging, plasma markers and autopsy data uncover a specific rostral locus coeruleus vulnerability to hyperphosphorylated tau

Maxime Van Egroo^{1,2,3} , Joost M. Riphagen^{2,3} , Nicholas J. Ashton^{4,5,6,7}, Shorena Janelidze⁸, Reisa A. Sperling^{3,9,10}, Keith A. Johnson^{2,3,10} , Hyun-Sik Yang^{3,9,10} , David A. Bennett¹¹, Kaj Blennow^{4,12} , Oskar Hansson^{8,13} , Henrik Zetterberg^{4,12,14,15,16} and Heidi I. L. Jacobs^{1,2,3}

© The Author(s) 2023

Autopsy data indicate that the locus coeruleus (LC) is one of the first sites in the brain to accumulate hyperphosphorylated tau pathology, with the rostral part possibly being more vulnerable in the earlier stages of the disease. Taking advantage of recent developments in ultra-high field (7 T) imaging, we investigated whether imaging measures of the LC also reveal a specific anatomic correlation with tau using novel plasma biomarkers of different species of hyperphosphorylated tau, how early in adulthood these associations can be detected and if are associated with worse cognitive performance. To validate the anatomic correlations, we tested if a rostro-caudal gradient in tau pathology is also detected at autopsy in data from the Rush Memory and Aging Project (MAP). We found that higher plasma measures of phosphorylated tau, in particular ptau₂₃₁, correlated negatively with dorso-rostral LC integrity, whereas correlations for neurodegenerative plasma markers (neurofilament light, total tau) were scattered throughout the LC including middle to caudal sections. In contrast, the plasma A β _{42/40} ratio, associated with brain amyloidosis, did not correlate with LC integrity. These findings were specific to the rostral LC and not observed when using the entire LC or the hippocampus. Furthermore, in the MAP data, we observed higher rostral than caudal tangle density in the LC, independent of the disease stage. The in vivo LC-phosphorylated tau correlations became significant from midlife, with the earliest effect for ptau₂₃₁, starting at about age 55. Finally, interactions between lower rostral LC integrity and higher ptau₂₃₁ concentrations predicted lower cognitive performance. Together, these findings demonstrate a specific rostral vulnerability to early phosphorylated tau species that can be detected with dedicated magnetic resonance imaging measures, highlighting the promise of LC imaging as an early marker of AD-related processes.

Molecular Psychiatry (2023) 28:2412–2422; <https://doi.org/10.1038/s41380-023-02041-y>

INTRODUCTION

Alzheimer's disease (AD) pathogenesis starts two to three decades before the emergence of clinical symptoms [1]. Recognition of this protracted involvement of the disease along with the observation that clinical trials targeting patients in the prodromal or later stages of the disease have not successfully resulted in functional changes, underscore the importance of detecting and implementing interventions for AD at a much earlier asymptomatic stage [2, 3]. In the search for the earliest and meaningful markers of AD-related changes, the brainstem locus coeruleus (LC) has attained significant attention [4].

Autopsy studies reported accumulation of hyperphosphorylated tau in the LC starting as early as age 20 [5, 6]. Detecting tau in the LC using current positron emission tomography (PET) ligands is arduous given the off-target binding to neuromelanin cells that also accumulate in the LC [7–9]. But, developments in MRI methods have enabled the localization of the LC in vivo [10], and work by our group indicated that the LC MRI-signal can convey information related to tau and risk of AD [11, 12]. We demonstrated that lower MRI-based LC integrity measures correlate with greater tau deposition in early cortical regions in

¹Faculty of Health, Medicine and Life Sciences, School for Mental Health and Neuroscience, Alzheimer Centre Limburg, Maastricht University, Maastricht, The Netherlands. ²Gordon Center for Medical Imaging, Department of Radiology, Massachusetts General Hospital, Boston, MA, USA. ³Harvard Medical School, Boston, MA, USA. ⁴Department of Psychiatry and Neurochemistry, Institute of Neuroscience and Physiology, The Sahlgrenska Academy at the University of Gothenburg, Mölndal, Sweden. ⁵Centre for Age-Related Medicine, Stavanger University Hospital, Stavanger, Norway. ⁶King's College London, Institute of Psychiatry, Psychology and Neuroscience, Maurice Wohl Institute Clinical Neuroscience Institute, London, UK. ⁷NIHR Biomedical Research Centre for Mental Health and Biomedical Research Unit for Dementia at South London and Maudsley NHS Foundation, London, UK. ⁸Clinical Memory Research Unit, Department of Clinical Sciences Malmö, Lund University, Lund, Sweden. ⁹Center for Alzheimer Research and Treatment, Department of Neurology, Brigham and Women's Hospital, Boston, MA, USA. ¹⁰Department of Neurology, Massachusetts General Hospital, Boston, MA, USA. ¹¹Department of Neurological Sciences, Rush Alzheimer's Disease Center, Rush University Medical Center, Chicago, IL 60612, USA. ¹²Clinical Neurochemistry Laboratory, Sahlgrenska University Hospital, Mölndal, Sweden. ¹³Memory Clinic, Skåne University Hospital, Malmö, Sweden. ¹⁴Department of Neurodegenerative Disease, UCL Institute of Neurology, Queen Square, London, UK. ¹⁵UK Dementia Research Institute at UCL, London, UK. ¹⁶Hong Kong Center for Neurodegenerative Diseases, Clear Water Bay, Hong Kong, China.

[✉]email: [hjacobsm@mgh.harvard.edu](mailto:hjacobs@mgh.harvard.edu)

Received: 15 September 2022 Revised: 15 March 2023 Accepted: 17 March 2023

Published online: 5 April 2023

clinically normal individuals starting approximately 54 years of age. In addition, at subthreshold levels of β -amyloid ($A\beta$)-PET, we observed a steeper decline in memory for individuals with lower LC integrity as compared to those with higher LC integrity, demonstrating a synergistic effect of LC integrity and early AD pathology on downstream clinical symptoms [11].

Importantly, postmortem work indicated that the rostral and middle sections of the LC are possibly susceptible to volume loss at an earlier stage in the disease than the caudal section of the LC [13]. Because the LC does not undergo significant neuronal loss before Braak stage IV [13], this suggests that these volumetric differences may be tau related [14]. Accordingly, recent 3 T MRI studies also reported that lower integrity in the rostral section of the LC correlated with memory decline, lower cortical thickness and greater risk of mild cognitive impairment (MCI) [15–17]. However, there is inconsistent data on the relationship between tau-PET and regional LC integrity. A study combining data from healthy controls, MCI and AD patients, showed that lower middle-caudal LC integrity was associated with greater temporal lobe MK-6240 tau-PET burden [18]. On the other hand, lower rostral-middle LC integrity in a group of autosomal dominant Alzheimer's disease (ADAD) patients (symptomatic and asymptomatic) was associated with greater occipito-temporo-parietal FTP-PET burden [19]. These inconsistencies may be due to the merging of distinct disease stages, a more accelerated disease progression in ADAD [12], or the use of different tau-tracers. Even though MK-6240 is presumed to signal earlier tau aggregations than the FTP tracer, both tracers are less sensitive to earlier non-fibrillar forms of tau [20].

New advances in fluid biomarkers can act as proxies for soluble tau originating from the central nervous system, ushering a new era for the early detection of AD. Based on postmortem and the available imaging data, we hypothesized that specifically the rostral part of the LC would be vulnerable to early AD tau-related processes. This hypothesis can now be evaluated by taking advantage of exciting developments in fluid biomarkers using high sensitivity immunoassay technologies that resulted in several well-validated and robust plasma markers of neurodegeneration (neurofilament light (NFL), total tau [21, 22], β -amyloid ($A\beta$) and various hyperphosphorylated tau (ptau) species [23]. Plasma ptau epitopes (ptau₁₈₁, ptau₂₁₇, ptau₂₃₁) levels are concordant with autopsy findings, have high sensitivity and specificity to detect tau-pathology on PET, and increase early in the preclinical stage of AD [24–27]. In particular, ptau₂₃₁ associated more robustly with tau-PET in asymptomatic individuals and was able to differentiate PET Braak stage 0 from Braak stage I/II and detect incipient amyloid pathology [28–30].

To examine regional vulnerability within the LC, it is important to consider that 3 T MRI methods acquire the LC in anisotropic voxels size (i.e. 0.3x0.3x3mm), which are often resampled to isotropic resolution. Such procedures can introduce noise and distortions in small regions such as the LC. Our efforts in 7 T MRI now provide a unique, detailed window in localization and anatomy of the LC at 0.4 mm near-isotropic voxel size [31, 32]. Here, we related LC integrity using 7 T MRI to different AD plasma markers in asymptomatic individuals across a wide age range, including individuals with preclinical AD. We then examined whether LC integrity and plasma markers are interactively or independently associated with cognition. To validate our in vivo findings, we also compared the proportion of neurons that were tau-positive in the rostral LC versus those in the caudal LC in 77 autopsy cases from the Rush Memory and Aging Project (MAP).

MATERIALS AND METHODS

Participants

The 7T dataset. Cognitively unimpaired individuals (age range = 30–85, 52 females (52.50%)) were recruited from the general community in the

most Southern region of the Netherlands. All participants were screened to exclude a history of major psychiatric or neurological disorders, having a history of brain injury of brain surgery, taking medications that may influence cognitive functioning, or being not eligible for ultra-high field MRI-scanning. To exclude individuals with depressive symptoms, we screened all participants using the Hamilton Rating Scale for Depression (all within normal range = 0–12; mean \pm SD = 2.23 \pm 2.53). All participants received monetary compensation and provided written informed consent. Approval of the experimental protocol was obtained from the local ethical committee of the Faculty of Health, Medicine and Life Sciences at Maastricht University, The Netherlands.

The MAP dataset. The dataset included 77 participants from the Rush Memory and Aging Project (MAP), an ongoing longitudinal clinical-pathologic studies that started in 1997 [33, 34]. Eligibility criteria included age > 55 years, absence of a previous dementia diagnosis and consent to annual clinical evaluation and brain autopsy at death. Participants were recruited from retirement communities, social service agencies and subsidized housing facilities, and individual homes in the Chicago metropolitan region. This sample included individuals for whom detailed LC neuropathology data was available and consisted of individuals with normal cognition ($n = 29$), mild cognitive impairment (MCI) ($n = 27$) or AD ($n = 21$) at their last clinical visit prior to autopsy. Diagnosis was done each year by a neuropsychologist and clinician, and final diagnosis was by a neurologist blinded to postmortem data, based on the National Institute of Neurological and Communicative Disorders and Stroke and the AD and Related Disorders Association (NINCDS/ADRDA) criteria [35–37]. The average time interval between last visit and death for these participants was 0.77 years (SD = 0.60). All data were de-identified and shared with a Data User Agreement. The study was approved by an institutional review board of Rush University Medical Center. All participants signed an informed consent, an Anatomical Gift Act, and a repository consent which allowed their data to be shared.

Structural magnetic resonance imaging (7 T dataset)

MRI data acquisition. MR scans were performed in a 7 T Magnetom Siemens (Siemens Healthineers, Erlangen, Germany) with a 32-channel head coil (Nova Medical, Wilmington, MA, USA). First, we acquired a Magnetization Prepared 2 Rapid Acquisition Gradient Echoes (MP2RAGE) sequence [38] for whole brain imaging (TR = 5000 ms, TE = 2.47 ms, flip angle = 5°/3°, voxel size = 0.7 \times 0.7 \times 0.7 mm³, number of slices = 240). An in-house developed magnetization transfer-weighted turbo flash (MT-TFL) sequence [31] was performed to image the LC at high resolution. The sequence consisted of a multi-shot 3D-readout (TR = 538 ms, TE = 4.08, flip angle = 8°, voxel size = 0.4 \times 0.4 \times 0.5 mm³, number of slices = 60) with center-out k-space sampling, preceded by 20 long off-resonant Gaussian sinc pulses (pulse length = 5.12 ms, bandwidth = 250 Hz, B₁ = 0.25 μ T). For the MT-TFL sequence, the field-of-view was placed perpendicular to the pons and covered the area between the inferior colliculus and the inferior border of the pons.

MRI data processing. The MP2RAGE images were processed with FreeSurfer v6.0.0 (<https://surfer.nmr.mgh.harvard.edu>) using the software package's automated reconstruction protocol as described previously, including expert options for 7 T images [39]. Briefly, each T1-weighted image was subjected to an automated segmentation process involving intensity normalization, skull stripping, segregating left and right hemispheres, removing brainstem and cerebellum, correcting topology defects, defining the borders between gray/white matter and gray/cerebrospinal fluid, and parcellating cortical and subcortical areas. We visually inspected and, if necessary, edited each image. As a control measure for the LC, we extracted the bilateral hippocampal volume and adjusted it for intracranial volume (eTIV) using the following equation [40]:

$$\text{Adjusted hippocampal volume} = \text{raw hippocampal volume} - b(\text{eTIV} - \text{Mean eTIV})$$

where b indicates the regression coefficient when raw hippocampal volume is regressed against eTIV.

The MT-TFL images were intensity-normalized in a slice-specific manner using the subject-specific mean intensity of a 10 \times 10 voxel region-of-interest located in the pontine tegmentum (PT). From these images, a study-specific template of the LC scans was created with an iterative diffeomorphic warp estimate using the `buildtemplateparallel.sh` script of

ANTS, as described previously [32, 41]. The LC was manually delineated on the common space twice by an expert (HJ, spatial correlation $r = 0.90$) and by another rater (spatial correlation between raters $r = 0.83$), guided by the voxel intensities and known LC anatomy. This segmented LC mask was applied to the high-resolution individual spatial and intensity-normalized LC images (Supplemental Fig. 1). From the template we constructed a surface rendering for visualization purposes of our results. To show regional specificity, we also extracted intensity values from the entire LC. Using the inverse warp, we further obtained subject-specific LC segmentations, extracted the bilateral LC volume and adjusted it for eTIV for control analyses.

Plasma markers (7T dataset)

Fasted EDTA plasma samples were obtained through venipuncture from the antecubital vein and processed according to the SOP stipulated by the central biobank of Maastricht University Medical Center. Samples were centrifuged at $2000 \times g$, aliquoted in polypropylene tubes, and stored at -80°C in our biobank within 60 min of collection. Plasma biomarkers were analyzed in randomized order using ultra-sensitive Single molecule array (Simoa) assays (Quanterix, Inc) for $\text{A}\beta_{42}$ and $\text{A}\beta_{40}$ (to create $\text{A}\beta_{42/40}$ ratio), total tau (Neurology 3-Plex A Advantage Kit), ptau₁₈₁ (pTau-181 V2 Advantage Kit), ptau₂₃₁ (University Gothenburg) [28] and NFL (NF-light™ Advantage Kit) at the University of Gothenburg (Sweden). Analyses were performed in duplicates using a 1:4 automated dilution protocol for all markers, except for 1:2 dilution protocol for ptau₂₃₁. Analysis of plasma ptau₂₁₇ was performed at Lund University (Sweden) using the Meso Scale Discovery (MSD) platform as previously described [24]. The range of values measured is consistent with other studies examining similar cohorts (Table accompanying Supplemental Fig. 3). Based on a previously defined cut-off ($\text{A}\beta_{42/40}$ ratio = 0.080 [30]) in an asymptomatic cohort using the same assay in the same lab (University Gothenburg) we identified 20 $\text{A}\beta +$ individuals. *APOE* genotyping was performed using polymerase chain reaction based on blood sample DNA extraction. Participants' *APOE* status was defined as 'ε4 carrier' if they carry at least one ε4 allele. 48.5% ($n = 48$) carried at least one ε4 allele and/or has elevated plasma $\text{A}\beta_{42/40}$ values, and hence can be considered at-risk of developing AD. Technicians handling the blood samples were blinded to the participant, cognitive and imaging data, and staff collecting cognitive or imaging data were blinded to blood results.

Neuropathological measures (MAP dataset)

Immediately after participants' death, brains were extracted, weighed, and the brainstem and cerebellar hemispheres removed. Both hemispheres and the brainstem were sectioned into 1 cm-thick coronal slabs. One hemisphere was frozen as were select samples of the brainstem; the remained was fixed in 4% paraformaldehyde. The average postmortem time was 7.09 h (SD:3.89 h). Neuronal density (per mm^2) and paired helical filaments (PHF) tau tangle density of the LC were examined using immunohistochemistry with a monoclonal anti-tyrosine hydroxylase antibody and an anti-paired helical filaments tau antibody AT8, respectively, each bilaterally at two levels of the LC (rostral-to-middle ("rostral") and main body or middle-to-caudal ("caudal")) [42, 43]. To allow for unbiased comparisons, we divided tangle density by the neuronal density for each section of the LC. We selected participants who had neuropathologic data on both sections of the LC ($n = 77$).

Cortical $\text{A}\beta$ load was quantified as percent area occupied by $\text{A}\beta$, labeled with a N-terminal directed monoclonal antibody, which identifies both the 1–40 and 1–42 length $\text{A}\beta$ fragments, while cortical PHF tau tangles, were quantified as the density of paired helical filament tau tangles with an antibody specific for phosphorylated tau, AT8 (density per square millimeter) across 8 regions [12]. Modified Bielschowsky silver quantification was used for Braak scoring of neurofibrillary pathology and Consortium to Establish a Registry for AD (CERAD) scoring of neuritic plaques. Using this information, the likelihood of AD pathology was identified according to the modified National Institute of Aging (NIA)-Reagan diagnosis of AD and grouped into not present (no or low likelihood) and present (intermediate and high likelihood). This evaluation is performed independent of clinical information, including the diagnosis [37, 44].

Neuropsychological assessment (7T dataset)

The preclinical Alzheimer's cognitive composite (PACC) was designed to be sensitive to cognitive change among individuals with preclinical AD, and consists of the average of z-transformed scores on the Mini-Mental-State

Examination, Logical Memory Delayed recall test, Digit Symbol Substitution Test, Free and Cued Selective Reminding test (free and total recall) and was later expanded to also include the category fluency [45]. We created a PACC-score based on the average of the z-scores of the performance on cognitive tests available in this cohort: Mini-Mental-State Examination, Digit Symbol Substitution Test, Rey-Auditory Verbal Learning Test (total and delayed free recall) and the category fluency test. Other collected behavioral measures were not analyzed for this study.

Statistical analyses

Statistical analyses were performed in R (version 4.1.2, <http://www.r-project.org/>). Group characteristics are represented in mean and standard deviation. Associations between the plasma markers, and age, sex, or *APOE*-status were examined with robust regression using the Huber M estimator. Robust regression is suited to handle outliers that are often observed in the skewed distributions of biomarker data. It effectively downweights their influence on the coefficients and regression fit and therefore, allows including individuals with more extreme (or abnormal) values, who are less prevalent in healthy populations but reflect the normal population. Voxel-wise robust regressions between LC intensity and each plasma marker, or their interactive or additive effects with plasma $\text{A}\beta_{42/40}$ were corrected for age, sex and *APOE*-ε4 status and adjusted for multiple testing using the probabilistic Threshold Free Cluster Enhancement at two-sided $p < 0.001$ per analysis (not across analyses). From each plasma marker cluster on the LC surface, we extracted subject-specific LC intensity values for further analyses. These plasma-based analyses were repeated for the entire LC intensity, bilateral LC volume, and hippocampal volume to examine the specificity of our findings. To examine whether associations between the plasma markers and LC intensity in their respective clusters occurred within a specific age-range, we ran sliding window analyses with 20-year age bins with bootstrapped 95% confidence intervals (5,000 iterations) [46]. Finally, using robust regression we examined whether the plasma markers that were significant from the previous analyses and the extracted LC intensity from the plasma-specific clusters were interactively or independently associated with PACC performance, with age, sex, education and *APOE*-ε4 status as covariates. We adjusted here for multiple testing using Bonferroni correction. Using the Johnson-Neyman approach we determined at which value the plasma marker modified the relationship between LC intensity and PACC. The threshold for statistical significance was set at two-sided $p < 0.05$, unless otherwise specified.

For the MAP dataset, we performed a repeated measures ANOVA with proportion of tangles in each section of the LC as within-subject factor, and age, sex, *APOE*-ε4 status, and postmortem interval as covariates. To test if these effects are independent of AD pathology, we also added cortical $\text{A}\beta$ or NIA-Reagan diagnosis of AD groups as covariate. In the second step, we included diagnosis (i.e., cognitively unimpaired, MCI or AD) as between-subject factor and interactions with LC sections, to determine whether the regional distribution of the proportion of LC tangles varied as a function of disease stage. Post-hoc adjustment for multiple comparisons was performed with Tukey's HSD.

RESULTS

Participant characteristics

In the 7T dataset, the mean age of the participants was 59.93 years (range 30–85 years), 52 were female (52.50%) and 37 (37%) carried at least one *APOE*-ε4 allele (Table 1). All participants were cognitively healthy (mean MMSE-score:28.98). In the MAP sample, the mean age of the participants was 88.59 years, 56 were female (72.72%), 10 carried at least one *APOE*-ε4 allele (13%), and 47 individuals (61%) showed evidence of AD pathology at autopsy according to the NIA-Reagan AD criteria. Histograms depicting age distributions of each cohort are provided in Supplemental Fig. 2

Correlations of plasma biomarkers with demographics

First-order correlations between all the plasma markers, and age, sex or *APOE* are shown in Supplementary Tables 1, 2 and Supplemental Fig. 3. In the following analyses, age analyses were adjusted for sex, and the sex analyses were adjusted for age. Older age was associated with lower $\text{A}\beta_{42/40}$ ($t = -4.63$, $p < 0.001$) and higher ptau₁₈₁ ($t = 3.25$, $p = 0.002$) and NFL ($t = 9.67$, $p < 0.001$). We detected no age-relationship for total tau ($t = -1.73$, $p = 0.08$),

Table 1. Participant characteristics.

	7 T dataset (N = 99)		MAP-study (N = 77)
Age (years)	59.93 (13.13)	Age (years)	88.59 (5.84)
Female (n, %)	52 (52.50%)	Female (n, %)	56 (72.72%)
Education (years)	14.44 (2.14)	Education (years)	14.44 (2.66)
MMSE (score)	28.98 (1.13)	MMSE (score)	23.52 (6.93) [§]
PACC (score)Range:	0.001 (0.67) –1.84–1.53		
APOE ϵ 4 (n, %)	37 (37.37%)	APOE- ϵ 4 (n, %)	10 (12.99%)
		Diagnosis (n, %)	29 CN (37.66%) 27 MCI (35.06%) 21 AD (27.27%)
		AD present (NIA-Reagan AD) (n, %)	47 (61.04%)
A β _{42/40}	0.09 (0.01)	Cortical A β	4.82 (4.58)
ptau ₁₈₁ (pg/ml)	1.67 (0.72)	Cortical tangles	5.35 (5.34)
ptau ₂₁₇ (pg/ml)	0.27 (0.11)		
ptau ₂₃₁ (pg/ml)	8.55 (3.82)		
Total tau (pg/ml)	2.65 (0.89)		
NfL (pg/ml)	18.28 (7.05)		
Adjusted hippocampus volume (mm ³)	6523.63 (673.76)		
LC intensity (a.u.) [#]	0.15 (0.06)	Relative LC tangles [#]	0.12 (0.14)

Demographics are presented in mean, standard deviation, or proportion. §:missing data for $n = 5$; #: these values are based on the entire LC.

MMSE Mini-Mental State Examination, PACC Preclinical Alzheimer's disease cognitive composite, CN cognitively normal, MCI mild cognitive impairment.

ptau₂₁₇ ($t = 0.40$, $p = 0.69$) or ptau₂₃₁ ($t = 1.17$, $p = 0.25$). Very weak or a lack of significant correlations between the ptau markers and A β _{42/40} has been reported in similar cohorts [30]. Females exhibited higher total tau ($t = -2.23$, $p = 0.023$), while males displayed higher ptau₁₈₁ ($t = 3.21$, $p = 0.002$). These sex differences remained significant when controlling for APOE- ϵ 4 status and A β _{42/40} ($t = -2.22$, $p = 0.03$ and $t = 3.82$, $p = 0.003$, respectively). There were no sex differences in A β _{42/40} ($t = 0.22$, $p = 0.83$), NfL ($t = 0.47$, $p = 0.64$), ptau₂₁₇ ($t = -0.81$, $p = 0.43$) or ptau₂₃₁ ($t = 1.47$, $p = 0.15$). Those who carry at least one ϵ 4 allele displayed lower A β _{42/40} ($t = -2.27$, $p = 0.025$). We observed no differences between ϵ 4-carriers and non-carriers for other biomarkers (total tau: $p = 0.79$, NfL: $p = 0.95$, ptau₁₈₁: $p = 0.18$, ptau₂₁₇: $p = 0.15$, ptau₂₃₁: $p = 0.66$, Fig. 1).

Voxel-wise relationships between locus coeruleus intensity and plasma biomarkers

Age, sex and APOE- ϵ 4 status were included as covariates in the voxel-wise regression analyses, given their significant associations with the plasma biomarkers. Voxel-wise analyses revealed that higher ptau₂₃₁ was associated with lower LC intensity in bilateral dorso-rostral clusters ($p_{TFCE} < 0.001$). Ptau₂₃₁ had the largest cluster-size (160 voxels). Ptau₁₈₁ (44 voxels), ptau₂₁₇ (37 voxels) and t-tau (49 voxels) correlated negatively with LC intensity in right dorso-rostral clusters. Small clusters of negative associations between LC intensity and NfL (51 voxels) were distributed across the length of the LC, and more prominent in the middle-to-caudal part. LC intensity was not associated with A β _{42/40} (Fig. 2). Adjusting for A β _{42/40} did not change these associations. We did not find interactions between A β _{42/40} and any of the other plasma markers on LC intensity. Consistent with this, we observed similar negative slopes between the ptau markers, in particular the ptau₂₃₁, and intensity in the LC clusters across A β + and A β -groups (Supplemental Fig. 4). The control brain measures, hippocampal volume, bilateral LC volume, and average entire LC intensity, were not associated with any of the plasma markers (Supplemental Table 3).

Age-window of the relationship between locus coeruleus intensity and plasma biomarkers

Bootstrapped sliding window analyses showed that the relationship between ptau₁₈₁ and LC intensity in its cluster was significant for individuals older than 60 (Fig. 3A), for ptau₂₁₇ starting from 60.5 years (Fig. 3B), and for ptau₂₃₁ the relationship with LC intensity was significant from 55.5 years and older (Fig. 3C). Of the individuals older than 55.5 years, 41% (25/61) was considered at increased risk for AD-related processes based on A β < 0.08 or presence of at least one APOE ϵ 4 allele. For NfL and total tau, no robust age windows were detected. We confirmed these patterns in voxel-wise sliding window analyses: associations between ptau₁₈₁ and rostral dorsal LC intensity emerged in the early 60 s, while for ptau₂₁₇, we detected clusters in the dorsal rostral-middle LC from the early-mid 60 s. The earliest age-associations with LC intensity were found for ptau₂₃₁, revealing an anatomic pattern in the ventral and dorsal rostral parts of the LC starting from late 40 s and later associations (60's) in the middle-caudal section of the LC (Fig. 3A–C).

Independent and interactive relationships of plasma biomarkers and LC intensity on PACC

Based on the previous results, we focused the cognitive analyses on the ptau biomarkers. The interaction between ptau₁₈₁ and its associated LC intensity cluster on PACC performance was significant at trend-level ($p = 0.06$). There were no independent effects of ptau₁₈₁ and LC intensity on PACC. We found no interactive or independent relationships of ptau₂₁₇ with LC intensity in predicting PACC performance (Supplemental Table 4). At higher levels of ptau₂₃₁, in particular above 15.69 pg/ml, lower LC intensity was associated with worse PACC performance ($p = 0.016$ or $p_{BONF} = 0.048$, Fig. 4).

Regional specificity of tau in the LC in the autopsy dataset

In the MAP dataset, normalized density of LC tangles in the rostral LC was significantly greater than those in the caudal LC ($F_{(1,72)} = 13.14$, $p < 0.001$). This difference remained present when

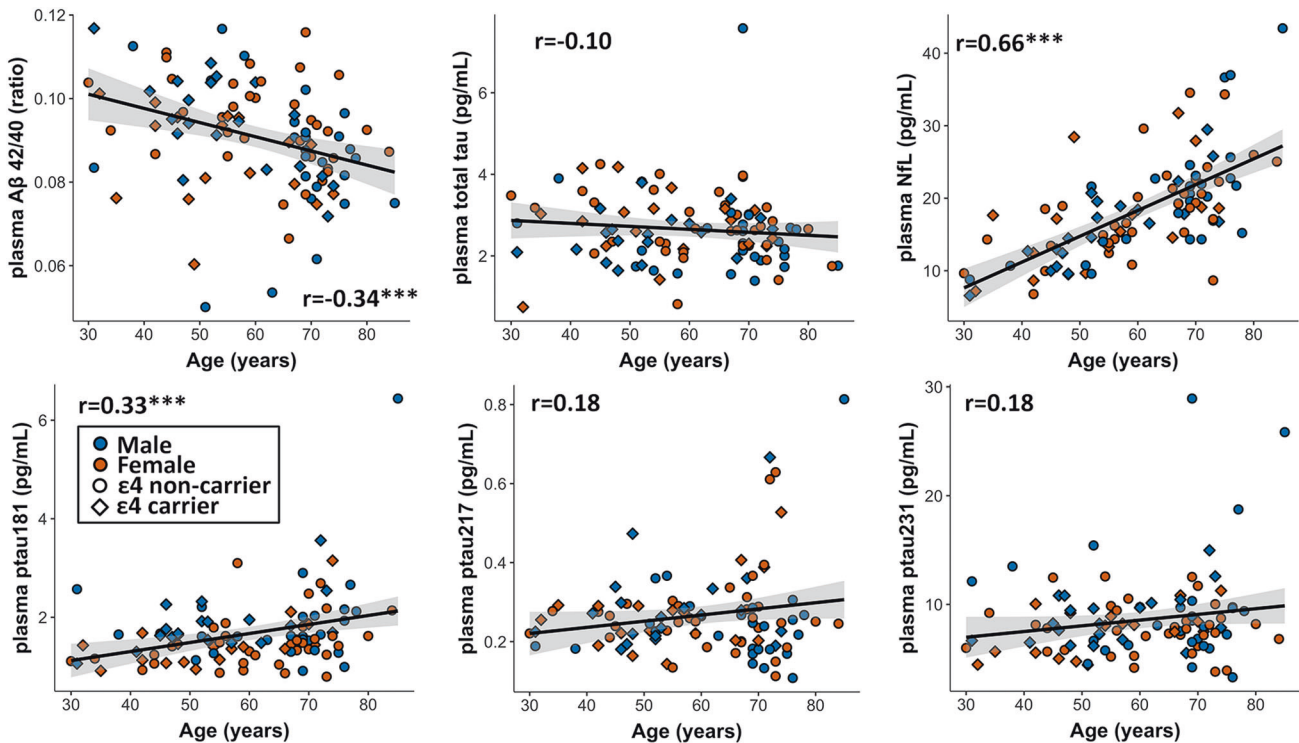


Fig. 1 Age-associations with the plasma biomarkers. Note: Correlations reflect the relationship between age and the plasma marker for the entire cohort. Males are indicated in blue, females in orange, $\epsilon 4$ non-carriers in circles and $\epsilon 4$ carriers in diamonds. Shaded region shows the 95% confidence interval of the regression fit (see also Supplementary Tables 1, 2 for all correlations in the entire sample and participants >50 years).

controlling for cortical A β ($F_{(1,71)}=13.39, p < 0.001$) or NIA-Reagan diagnosis of AD groups ($F_{(1,71)}=12.96, p < 0.001$, Fig. 5).

Upon examining the interaction between LC section and the diagnostic groups, we found no significant difference in rostral versus caudal LC tangle density across the groups ($F_{(1,70)}=0.07, p=0.94$, Supplemental Fig. 5). Across all groups, rostral LC tangle density was higher than caudal LC tangle density (contrast of main effect LC section: $\beta=0.50, t=2.21, p=0.031$; mean rostro-caudal LC tangle density difference for cognitively normal = 0.05 ± 0.13 , for MCI = 0.05 ± 0.09 and for AD = 0.05 ± 0.15).

DISCUSSION

As clinical trials targeting A β provided marginal clinical effects, the AD field has oriented its focus on earlier time windows in the disease process [3]. These earlier windows have compelled researchers to focus on tau pathology, which is more closely related to the emergence of clinical symptoms compared to A β [47, 48]. The LC is one of the earliest brain regions accumulating hyperphosphorylated tau [6] and recent work emphasized its potential as early marker of future AD-related processes, including tau and cognitive decline [11, 12, 17]. Here we aimed to examine whether different tau species and markers of neurodegenerations correlate to specific anatomic patterns of integrity within the LC across the adult lifespan. We found that lower integrity in bilateral dorso-rostral clusters of the LC was associated with greater ptau₂₃₁ concentrations, starting from midlife (~55 years). Higher ptau₂₁₇ and ptau₁₈₁ levels were associated with lower LC integrity in smaller right dorso-rostral clusters, starting from age 60. Similarly, the autopsy data revealed a higher tangle density in the rostral compared to the caudal part of the LC, independent of AD likelihood. Furthermore, lower PACC scores were associated with lower rostral LC integrity, particularly for individuals with higher plasma ptau₂₃₁. By contrast, higher NFL was associated with

predominantly lower middle-to-caudal LC integrity, independent of age. As tau phosphorylation at threonine 231 is one of the earliest events in the phosphorylation cascade hindering tubulin assembly [49], these findings illustrate that changes in rostral LC intensity can reflect processes related to very early tau aggregation, whereas integrity changes towards the caudal direction in the LC may reflect more nonspecific neurodegeneration.

The fine-grained topography of correlations between LC integrity and ptau markers, demonstrating a predilection of AD-related processes for rostral regions of the LC, is consistent with autopsy reports [13, 50]. Work by Theofilas and colleagues reported 8.40% volume loss – not neuronal loss – per Braak stage, starting in Braak stage 0 for the rostral and middle LC [13]. Consistent with our previous work [32] and with the observation that the caudal LC contains fewer AD-related changes [13], we found that indicators of nonspecific neurodegeneration were associated with lower caudal LC integrity. Ultra-high field imaging of the LC in Parkinson's disease reported lower integrity in the caudal part in patients compared to controls [51]. We speculate that these observations emphasize a rostro-caudal gradient of vulnerabilities to specific pathologic events within the LC that may also be disease-specific. In accordance with this hypothesis, we found that rostral-middle parts of the LC are more vulnerable to hyperphosphorylated tau whereas the caudal part may be more affected by non-specific neurodegeneration.

With respect to the plasma ptau epitopes, we found that ptau₂₃₁ was more robustly and earlier in life associated with LC integrity compared with the ptau₂₁₇ and ptau₁₈₁ markers. Neuropathology studies demonstrated that tau phosphorylation at threonine 231 may signal features of tau that precede the pre-neurofibrillary tangle [52] and reflect the earliest events in the phosphorylation cascade hindering tubulin assembly [49]. In the ALFA + cohort of asymptomatic individuals, ptau₂₃₁ changes preceded changes in other markers and predicted increases in A β -

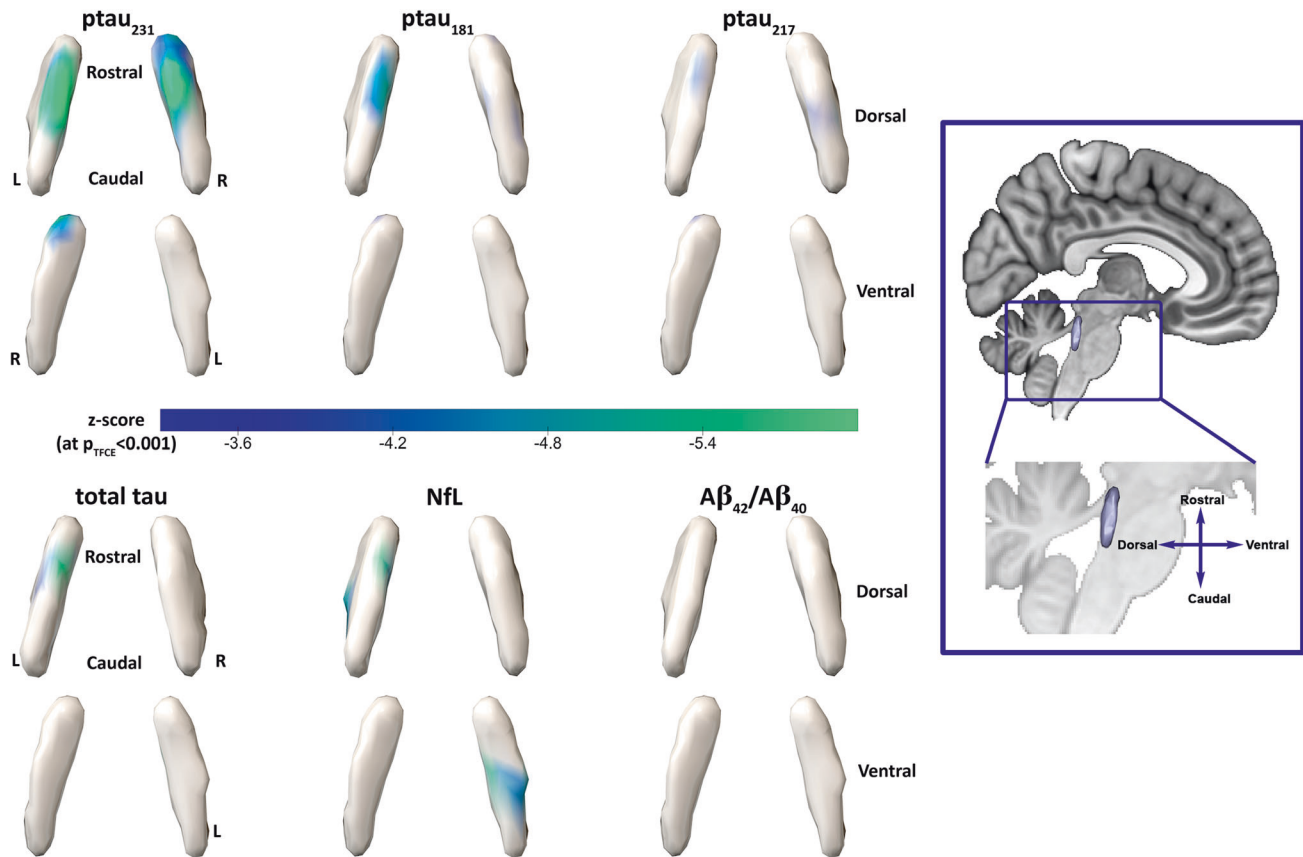


Fig. 2 Voxel-wise associations between LC intensity and the plasma markers. Note: Analyses were adjusted for age, sex, *APOE* ϵ 4 status and multiple comparisons using the threshold-free cluster enhancement approach (TFCE) at $p < 0.001$. Color scale shows the corresponding z-scores. The box on the right provides information for anatomical orientation of the LC surfaces. L = left, R = right.

PET burden among individuals with no PET-evidence of $A\beta$ -pathology as well as in the younger group (45–60 years) [30]. Given the concordance between these spatial patterns in the voxel-wise analyses and the higher rostral vulnerability in the autopsy data, our previous report on converging patterns of associations between LC integrity and tau-PET with autopsy data [11], and the similarities between our cohort and the ALFA + cohort, our findings here support the idea that LC integrity measures may capture very early aberrant tau-related processes [6, 53, 54].

The finding that $ptau_{231}$ may be an early marker fits with recent work showing that $ptau_{231}$ was able to differentiate between PET-derived Braak stage 0 and Braak stage I–II, whereas $ptau_{181}$ was not [28]. Furthermore, elevations in $ptau_{231}$ can be detected at lower amounts of AD-type pathology compared to $ptau_{181}$ [55]. Importantly, similar observations have been made for cerebrospinal fluid tau markers [56, 57]. Plasma $ptau_{181}$ correlates well with tau-PET, can detect elevated $A\beta$ -PET and discriminate AD patients from non-AD patients [25, 27]. Previous work demonstrated that plasma $ptau_{217}$ detects AD-related processes slightly earlier than $ptau_{181}$ as it was better in predicting elevated entorhinal tau [58]. We did not see a remarkable difference between the topography on the LC for $ptau_{217}$ and $ptau_{181}$. Furthermore, our sliding window analyses revealed a similar age-range (>60 years) during which both $ptau_{217}$ and $ptau_{181}$ have their strongest relationship with LC integrity. Our plasma $A\beta_{42/40}$ marker did not correlate with the tau markers, and this lack of correlations between the $A\beta$ and tau markers is consistent with observations in the ALFA + cohort [30]. Within the $A\beta+$ and $A\beta-$ groups, we observed similar associations between the tau markers and LC integrity, in particular for $ptau_{231}$, and we posit that these $ptau_{231}$ -related LC

changes may capture early processes on the AD pathophysiological continuum. Importantly, the sensitivity of detecting early tau-related LC changes is higher when honing in on the rostral LC instead of the entire average LC or LC volume. Furthermore, we did not observe tau-related associations with hippocampal volume, further emphasizing the specificity of the rostral LC as a potential marker to detect very early AD-related processes.

This rostro-caudal gradient of tau-related vulnerability within the LC also aligns with the topographic arrangement of axonal projections and the cytoarchitecture of the LC [14]. Projections of the LC are not randomly organized, as neurons in the rostro-middle sections of the LC preferentially project to the higher-order cognitive regions of the cortex, while the majority of the neurons in the caudal section of the LC projects to the cerebellum and spinal cord [59, 60]. Furthermore, the rostral and caudal parts of the LC have distinct cell types and cell sizes organized in clusters, supporting functional heterogeneity [61, 62]. The dorso-rostral LC contains almost uniquely densely packed small fusiform neurons, which have long, thin dendrites projecting to the hippocampus and cortex, and are more heavily pigmented and more vulnerable to pathology than the larger cells. The caudal part of the LC contains mostly large multipolar neurons [62–64]. This distribution may also support the rostral LC's critical contribution in modulating cognition, because fusiform neurons tend to have shorter action potentials with larger amplitudes compared to multipolar cells [65, 66]. These electrophysiological properties enable fusiform cells to sustain high frequency firing critical to focused attention, learning and responding to salient stimuli [61, 67].

Thus, the specific vulnerability of rostral neurons to hyperphosphorylated tau aggregation may affect the functioning of these

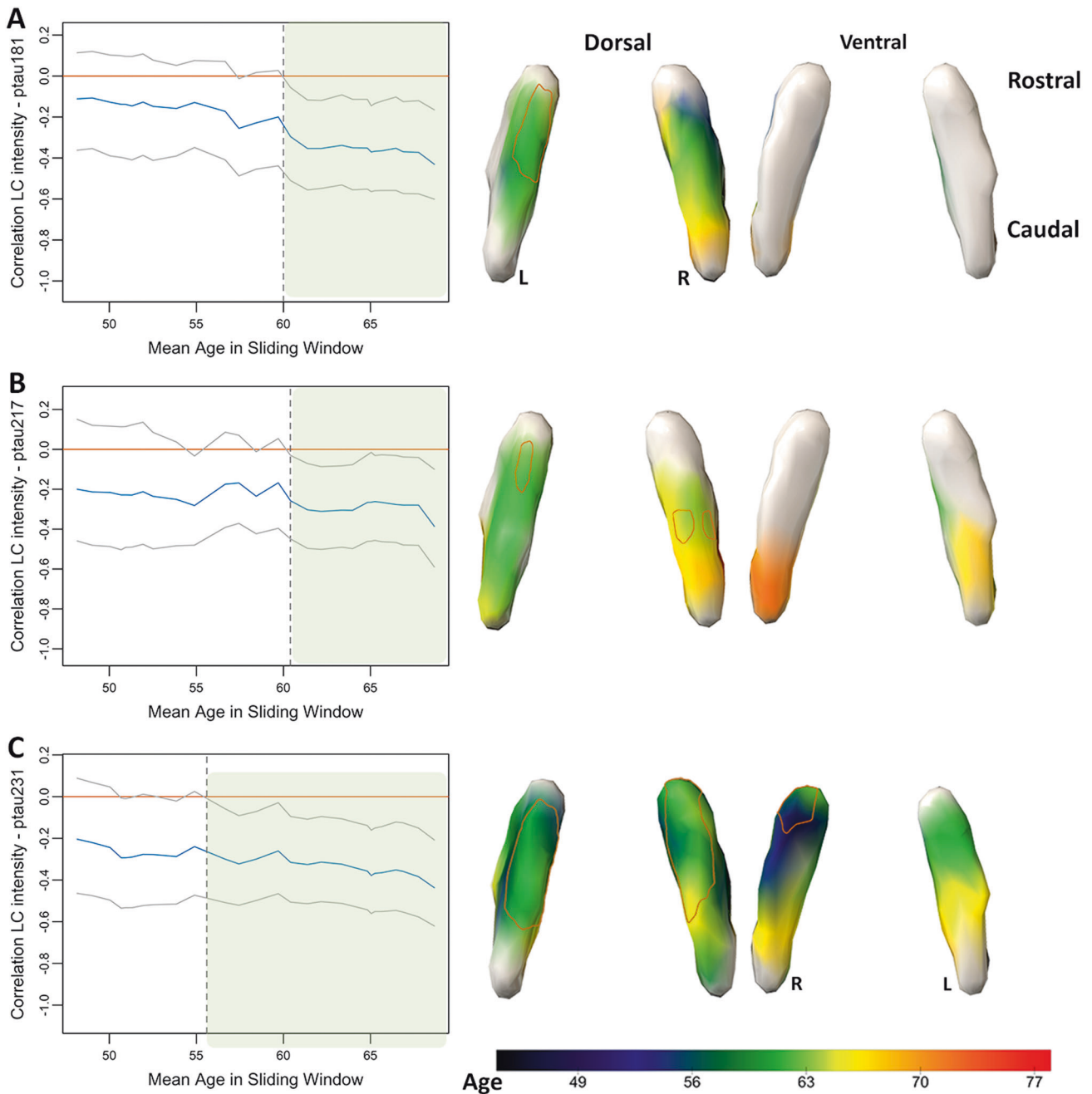


Fig. 3 Age-windows of associations between plasma markers and LC intensity. Note: Results of the bootstrapped sliding window analyses: blue line depicts the correlation coefficient between the plasma marker and the respective LC intensity cluster, the gray lines indicate the bootstrapped 95% confidence interval (5000 replicates at $p < 0.05$). Age window where the association was robustly significant is marked in the green shaded region with the starting age indicated by the dashed line. **A** Results for plasma ptau₁₈₁, **(B)** ptau₂₁₇ and **(C)** ptau₂₃₁. To map the anatomy of these associations, we also performed bootstrapped voxel-wise sliding window analyses examining the age-window of associations between regional LC intensity and each ptau marker (right column). The scale bar shows the age window where the associations were observed (cold (blue)): starting at younger ages; warm (orange): starting at older ages. White regions on the surface indicate voxels where no robust age-window was detected. The orange demarcation on the LC surfaces show the significant clusters observed in Fig. 2.

smaller cells and hence, affect its capacity to modulate cognition. Notably, of all three ptau markers, ptau₂₃₁ was also the only marker predicting PACC performance in interaction with rostral LC integrity, at a threshold value that was slightly higher than a recently published study reporting faster cognitive decline of unimpaired older individuals with elevated ptau₂₃₁ [68]. Furthermore, in populations consisting of unimpaired and impaired individuals higher ptau₂₃₁ was associated with faster decline on the MMSE, Dementia Rating Scale and Clinical Dementia Rating-

Sum of Boxes scale as compared to ptau₁₈₁ [28, 55]. These findings further confirm that lower rostral LC integrity measures can signal risk for early AD-related processes.

This study has several limitations. First, while this is currently the largest cohort using state-of-the-art 7T LC imaging, our sample size is moderately large. Due to the greater forces of the magnetic field, ultra-high field imaging has more strict inclusion criteria, resulting in lower enrollment and possibly a selection-bias to the healthier population. Second, due to the SARS-CoV-2

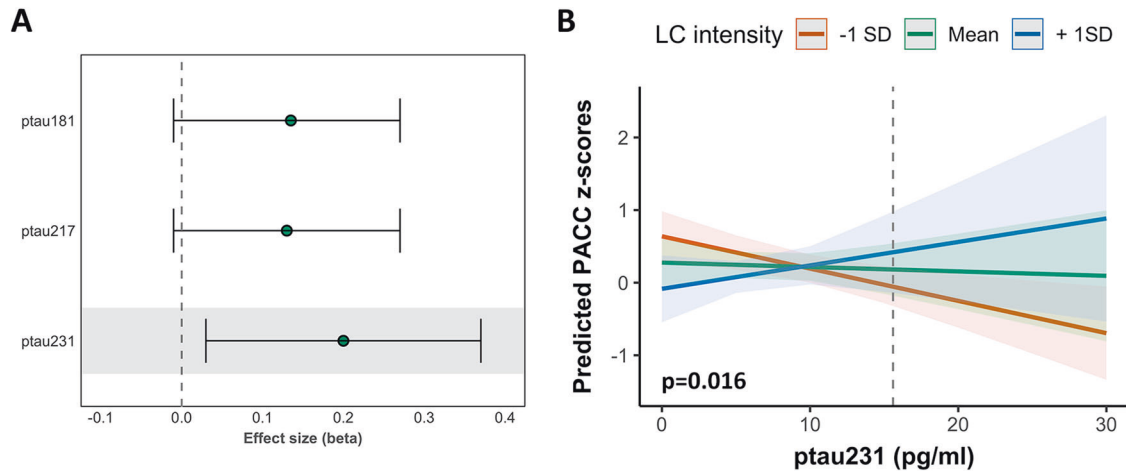


Fig. 4 Interactive relationships between LC intensity and plasma markers in predicting PACC performance. Note: **A** effect sizes and 95% confidence intervals of the interaction between each biomarker and the respective LC intensity cluster on PACC performance. The shaded region indicates the best model (ptau₂₃₁) and this association is depicted in **(B)**. **B** At values above ~15.7 pg/ml of ptau₂₃₁, lower LC integrity is associated with lower PACC score.

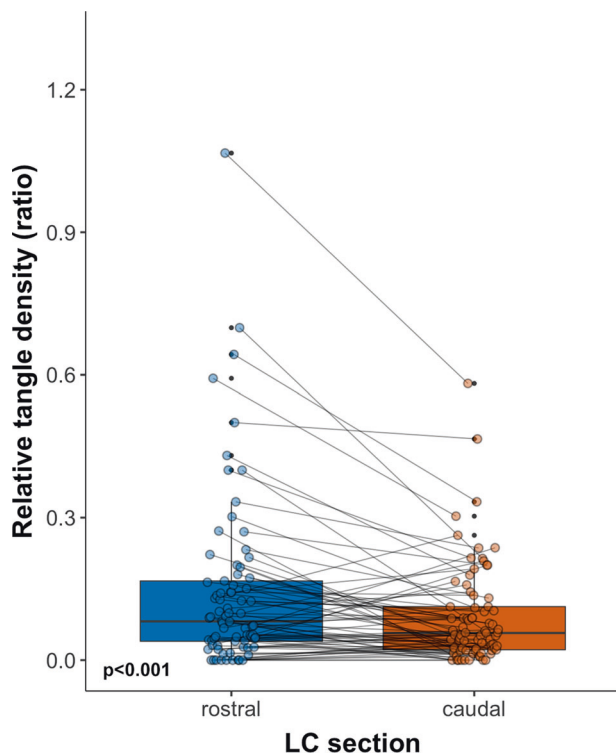


Fig. 5 Rostral versus caudal tangle density in the LC in the MAP dataset. Note: Boxplot depicting the rostral and caudal LC density (relative to its neuronal density) for the entire MAP sample (MAP dataset, $N = 77$). The boxplot depicts the interquartile interval (quartile one to three), with the horizontal line in the box representing the median.

pandemic longitudinal assessments were delayed, limiting our current analyses to the cross-sectional data. Therefore, it also remains uncertain whether these individuals will exhibit progression consistent with AD trajectories or primary age-related tauopathy (PART) [69]. As we do not have topographical information of tau and because we cannot preclude disease progression given that this sample is still cognitively unimpaired, making a distinction between these pathways is difficult. The fact that ptau₂₃₁ has shown to be a sensitive early marker of

underlying AD pathology [28], predicts accumulation of A β [30], that almost half of the individuals >55.5 years in whom we found ptau-LC associations has either a genetic risk factor for AD or presence of elevated A β , and that these associations are also detected in the A β + individuals separately, makes it more likely that our observations reflect AD-related pathways. Nonetheless, follow-up of these individuals will be required to describe their phenotypic trajectory. Given that our neuropathologic observations confirm a rostral vulnerability independent of disease stage, similar associations can be expected in impaired individuals. Third, caution is needed when interpreting the caudal LC. As this region of the LC is more diffuse [70], it is also more challenging to image it and the data acquired may therefore not capture the full length of the LC. Therefore, volumetric LC measures should also be interpreted with caution. Finally, comparisons between the three ptau epitopes need to take into account that these markers were quantified using different platforms and antibodies [58].

To conclude, the plasma ptau₂₃₁ marker is specifically associated with lower dorso-rostral LC integrity starting in midlife, and jointly, integrity of this LC section and plasma ptau₂₃₁ predict lower PACC performance. These findings link a plasma marker presumed to reflect a very early phase of hyperphosphorylation of tau specifically to the part of the LC exhibiting early vulnerability to tau deposition. Reductions in integrity of the dorso-rostral LC may thus signal very early AD risk, including early tau aggregation.

DATA AVAILABILITY

Participants in the 7T study did not explicitly consent to their data being made public. Requests for the anonymized data should be made to Dr. Heidi Jacobs (www.heidijacobs.org; h.jacobs@maastrichtuniversity.nl or hjacobs@mgh.harvard.edu) and will be reviewed by an independent data access committee, taking into account the research proposal and intended use of the data. Requestors are required to sign a data sharing agreement to ensure participants' confidentiality is maintained prior to release of any data and that procedures conform with the EU legislation on the general data protection regulation and local ethical regulations. Data domains in which human data collection is ongoing can only be shared under these regulations once data collection and quality assessment are completed. Data from ROSMAP is available upon request at <https://www.radc.rush.edu>.

REFERENCES

- Jack CR Jr, Knopman DS, Jagust WJ, Shaw LM, Aisen PS, Weiner MW, et al. Hypothetical model of dynamic biomarkers of the Alzheimer's pathological cascade. *Lancet Neurol*. 2010;9:119–28.

2. Sperling R, Mormino E, Johnson K. The evolution of preclinical Alzheimer's disease: implications for prevention trials. *Neuron*. 2014;84:608–22.
3. Sperling RA, Rentz DM, Johnson KA, Karlawish J, Donohue M, Salmon DP, et al. The A4 study: stopping AD before symptoms begin? *Sci Transl Med*. 2014;6:228fs213.
4. Ehrenberg AJ, Kelberman MA, Liu KY, Dahl MJ, Weinshenker D, Falgas N, et al. Priorities for research on neuromodulatory subcortical systems in Alzheimer's disease: Position paper from the NSS PIA of ISTAART. *Alzheimers Dement*. 2023. <https://doi.org/10.1002/alz.12937>
5. Braak H, Del Tredici K. Where, when and in what form does sporadic Alzheimer's disease begin? *Curr Opin Neurol*. 2012;25:708–14.
6. Braak H, Thal DR, Ghebremedhin E, Del Tredici K. Stages of the pathologic process in Alzheimer disease: age categories from 1 to 100 years. *J Neuropathol Exp Neurol*. 2011;70:960–9.
7. Lee CM, Jacobs HIL, Marquie M, Becker JA, Andrea NV, Jin DS, et al. 18F-Flortaucipir Binding in Choroid Plexus: Related to Race and Hippocampus Signal. *J Alzheimers Dis*. 2018;62:1691–702.
8. Marquie M, Normandin MD, Vanderburg CR, Costantino IM, Bien EA, Rycyna LG, et al. Validating novel tau positron emission tomography tracer [F-18]-AV-1451 (T807) on postmortem brain tissue. *Ann Neurol*. 2015;78:787–800.
9. Aguero C, Dhaynaut M, Normandin MD, Amaral AC, Guehl NJ, Neelamkangam R, et al. Autoradiography validation of novel tau PET tracer [F-18]-MK-6240 on human postmortem brain tissue. *Acta Neuropathol Commun*. 2019;7:37
10. Betts MJ, Kirilina E, Otaduy MCG, Ivanov D, Acosta-Cabrero J, Callaghan MF, et al. Locus coeruleus imaging as a biomarker for noradrenergic dysfunction in neurodegenerative diseases. *Brain*. 2019;142:2558–71.
11. Jacobs HIL, Becker JA, Kwong K, Engels-Dominguez E, Prokopiou PC, Papp KV, et al. In vivo and neuropathology data support locus coeruleus integrity as indicator of Alzheimer's disease pathology and cognitive decline. *Sci Transl Med*. 2021;13:eabj2511.
12. Jacobs HIL, Becker JA, Kwong K, Munera D, Ramirez-Gomez L, Engels-Dominguez N, et al. Waning locus coeruleus integrity precedes cortical tau accrual in preclinical autosomal dominant Alzheimer's disease. *Alzheimers Dement*. 2023;19:169–80.
13. Theofilas P, Ehrenberg AJ, Dunlop S, Di Lorenzo Alho AT, Nguy A, Leite REP, et al. Locus coeruleus volume and cell population changes during Alzheimer's disease progression: A stereological study in human postmortem brains with potential implication for early-stage biomarker discovery. *Alzheimers Dement*. 2017;13:236–46.
14. Gilvesy A, Husen E, Magloczky Z, Mihaly O, Hortobagyi T, Kanatani S, et al. Spatiotemporal characterization of cellular tau pathology in the human locus coeruleus-pericoeruleus complex by three-dimensional imaging. *Acta Neuropathol*. 2022;144:651–76.
15. Bachman SL, Dahl MJ, Werkle-Bergner M, Duzel S, Forlim CG, Lindenberger U, et al. Locus coeruleus MRI contrast is associated with cortical thickness in older adults. *Neurobiol Aging*. 2021;100:72–82.
16. Dahl MJ, Mather M, Duzel S, Bodammer NC, Lindenberger U, Kuhn S, et al. Higher rostral locus coeruleus density is associated with better memory performance in older adults. *Nat Hum Behav*. 2019;3:1203–14.
17. Elman JA, Puckett OK, Beck A, Fennema-Notestine C, Cross LK, Dale AM, et al. MRI-assessed locus coeruleus integrity is heritable and associated with multiple cognitive domains, mild cognitive impairment, and daytime dysfunction. *Alzheimers Dement*. 2021;17:1017–25.
18. Cassidy CM, Therriault J, Pascoal TA, Cheung V, Savard M, Tuominen L, et al. Association of locus coeruleus integrity with Braak stage and neuropsychiatric symptom severity in Alzheimer's disease. *Neuropsychopharmacology*. 2022;47:1128–36.
19. Dahl MJ, Mather M, Werkle-Bergner M, Kennedy BL, Guzman S, Hurth K, et al. Locus coeruleus integrity is related to tau burden and memory loss in autosomal-dominant Alzheimer's disease. *Neurobiol Aging*. 2021;112:39–54.
20. Gogola A, Minhas DS, Villemagne VL, Cohen AD, Mountz JM, Pascoal TA, et al. Direct Comparison of the Tau PET Tracers (18)F-Flortaucipir and (18)F-MK-6240 in Human Subjects. *J Nucl Med*. 2022;63:108–16.
21. Lewczuk P, Ermann N, Andreasson U, Schultheis C, Podhorna J, Spitzer P, et al. Plasma neurofilament light as a potential biomarker of neurodegeneration in Alzheimer's disease. *Alzheimers Res Ther*. 2018;10:71.
22. Ashton NJ, Leuzy A, Lim YM, Troakes C, Hortobagyi T, Hoglund K, et al. Increased plasma neurofilament light chain concentration correlates with severity of post-mortem neurofibrillary tangle pathology and neurodegeneration. *Acta Neuropathol Commun*. 2019;7:5.
23. Zetterberg H. Biofluid-based biomarkers for Alzheimer's disease-related pathologies: an update and synthesis of the literature. *Alzheimers Dement*. 2022;18:1687–93.
24. Janelidze S, Berron D, Smith R, Strandberg O, Proctor NK, Dage JL, et al. Associations of Plasma Phospho-Tau217 Levels With Tau Positron Emission Tomography in Early Alzheimer Disease. *JAMA Neurol*. 2021;78:149–56.
25. Janelidze S, Mattsson N, Palmqvist S, Smith R, Beach TG, Serrano GE, et al. Plasma P-tau181 in Alzheimer's disease: relationship to other biomarkers, differential diagnosis, neuropathology and longitudinal progression to Alzheimer's dementia. *Nat Med*. 2020;26:379–86.
26. Mattsson-Carlgren N, Janelidze S, Palmqvist S, Cullen N, Svenningsson AL, Strandberg O, et al. Longitudinal plasma p-tau217 is increased in early stages of Alzheimer's disease. *Brain*. 2020;143:3234–41.
27. Thijssen EH, La Joie R, Wolf A, Strom A, Wang P, Iaccarino L, et al. Diagnostic value of plasma phosphorylated tau181 in Alzheimer's disease and frontotemporal lobar degeneration. *Nat Med*. 2020;26:387–97.
28. Ashton NJ, Pascoal TA, Karikari TK, Benedet AL, Lantero-Rodriguez J, Brinkmalm G, et al. Plasma p-tau231: a new biomarker for incipient Alzheimer's disease pathology. *Acta Neuropathol*. 2021;141:709–24.
29. Tissot C, Therriault J, Kunach P, L Benedet A, Pascoal TA, Ashton NJ, et al. Comparing tau status determined via plasma pTau181, pTau231 and [(18)F]MK6240 tau-PET. *EBioMedicine*. 2022;76:103837.
30. Mila-Aloma M, Ashton NJ, Shekari M, Salvado G, Ortiz-Romero P, Montoliu-Gaya L, et al. Plasma p-tau231 and p-tau217 as state markers of amyloid-beta pathology in preclinical Alzheimer's disease. *Nat Med*. 2022;28:1797–801.
31. Privououlos N, Jacobs HIL, Ivanov D, Uludag K, Verhey FRJ, Poser BA. High-resolution in vivo imaging of human locus coeruleus by magnetization transfer MRI at 3T and 7T. *Neuroimage*. 2018;168:427–36.
32. Van Egroo M, van Hooren RWE, Jacobs HIL. Associations between locus coeruleus integrity and nocturnal awakenings in the context of Alzheimer's disease plasma biomarkers: a 7T MRI study. *Alzheimers Res Ther*. 2021;13:159.
33. Bennett DA, Schneider JA, Buchman AS, Barnes LL, Boyle PA, Wilson RS. Overview and findings from the rush Memory and Aging Project. *Curr Alzheimer Res*. 2012;9:646–63.
34. Bennett DA, Buchman AS, Boyle PA, Barnes LL, Wilson RS, Schneider JA. Religious orders study and rush memory and aging project. *J Alzheimers Dis*. 2018;64:S161–S189.
35. Bennett DA, Schneider JA, Aggarwal NT, Arvanitakis Z, Shah RC, Kelly JF, et al. Decision rules guiding the clinical diagnosis of Alzheimer's disease in two community-based cohort studies compared to standard practice in a clinic-based cohort study. *Neuroepidemiology*. 2006;27:169–76.
36. Bennett DA, Wilson RS, Schneider JA, Evans DA, Beckett LA, Aggarwal NT, et al. Natural history of mild cognitive impairment in older persons. *Neurology*. 2002;59:198–205.
37. Bennett DA, Schneider JA, Arvanitakis Z, Kelly JF, Aggarwal NT, Shah RC, et al. Neuropathology of older persons without cognitive impairment from two community-based studies. *Neurology*. 2006;66:1837–44.
38. Marques JP, Kober T, Krueger G, van der Zwaag W, Van de Moortele PF, Gruetter R. MP2RAGE, a self bias-field corrected sequence for improved segmentation and T1-mapping at high field. *Neuroimage*. 2010;49:1271–81.
39. Dale AM, Fischl B, Sereno MI. Cortical surface-based analysis. I. Segmentation and surface reconstruction. *Neuroimage*. 1999;9:179–94.
40. Jacobs HIL, Hedden T, Schultz AP, Sepulcre J, Perea RD, Amariglio RE, et al. Structural tract alterations predict downstream tau accumulation in amyloid-positive older individuals. *Nat Neurosci*. 2018;21:424–31.
41. Jacobs HIL, Privououlos N, Poser BA, Pagen LH, Ivanov D, Verhey FR, et al. Dynamic behavior of the locus coeruleus during arousal-related memory processing in a multi-modal 7T fMRI paradigm. *Elife*. 2020;9:e52059.
42. Buchman AS, Nag S, Shulman JM, Lim AS, VanderHorst VG, Leurgans SE, et al. Locus coeruleus neuron density and parkinsonism in older adults without Parkinson's disease. *Mov Disord*. 2012;27:1625–31.
43. Wilson RS, Nag S, Boyle PA, Hizez LP, Yu L, Buchman AS, et al. Neural reserve, neuronal density in the locus coeruleus, and cognitive decline. *Neurology*. 2013;80:1202–8.
44. Consensus recommendations for the postmortem diagnosis of Alzheimer's disease. The National Institute on Aging, and Reagan Institute Working Group on Diagnostic Criteria for the Neuropathological Assessment of Alzheimer's Disease. *Neurobiol Aging*. 1997;18:S1–2.
45. Papp KV, Rentz DM, Orlovsky I, Sperling RA, Mormino EC. Optimizing the preclinical Alzheimer's cognitive composite with semantic processing: The PACC5. *Alzheimers Dement (NY)*. 2017;3:668–77.
46. Bischof GN, Rodrigue KM, Kennedy KM, Devous MD Sr., Park DC. Amyloid deposition in younger adults is linked to episodic memory performance. *Neurology*. 2016;87:2562–6.
47. Bierer LM, Hof PR, Purohit DP, Carlin L, Schmeidler J, Davis KL, et al. Neocortical neurofibrillary tangles correlate with dementia severity in Alzheimer's disease. *Arch Neurol*. 1995;52:81–88.

48. Sanchez JS, Becker JA, Jacobs HIL, Hanseeuw BJ, Jiang S, Schultz AP, et al. The cortical origin and initial spread of medial temporal tauopathy in Alzheimer's disease assessed with positron emission tomography. *Sci Transl Med.* 2021;13:eabc0655.
49. Savastano A, Flores D, Kadavath H, Biernat J, Mandelkow E, Zweckstetter M. Disease-Associated Tau Phosphorylation Hinders Tubulin Assembly within Tau Condensates. *Angew Chem Int Ed Engl.* 2021;60:726–30.
50. German DC, Manaye KF, White CL 3rd, Woodward DJ, McIntire DD, Smith WK, et al. Disease-specific patterns of locus coeruleus cell loss. *Ann Neurol.* 1992;32:667–76.
51. O'Callaghan C, Hezemans FH, Ye R, Rua C, Jones PS, Murley AG, et al. Locus coeruleus integrity and the effect of atomoxetine on response inhibition in Parkinson's disease. *Brain.* 2021;144:2513–26.
52. Ercan-Herbst E, Ehrig J, Schondorf DC, Behrendt A, Klaus B, Gomez Ramos B, et al. A post-translational modification signature defines changes in soluble tau correlating with oligomerization in early stage Alzheimer's disease brain. *Acta Neuropathol Commun.* 2019;7:192.
53. Ehrenberg AJ, Nguy AK, Theofilas P, Dunlop S, Suemoto CK, Di Lorenzo Alho AT, et al. Quantifying the accretion of hyperphosphorylated tau in the locus coeruleus and dorsal raphe nucleus: the pathological building blocks of early Alzheimer's disease. *Neuropathol Appl Neurobiol.* 2017;43:393–408.
54. Chalermphanupap T, Weinschenker D, Rorabaugh JM. Down but Not Out: The Consequences of Pretangle Tau in the Locus Coeruleus. *Neural Plast.* 2017;2017:7829507.
55. Smirnov DS, Ashton NJ, Blennow K, Zetterberg H, Simren J, Lantero-Rodriguez J, et al. Plasma biomarkers for Alzheimer's Disease in relation to neuropathology and cognitive change. *Acta Neuropathol.* 2022;143:487–503.
56. Barthelemy NR, Li Y, Joseph-Mathurin N, Gordon BA, Hassenstab J, Benzinger TLS, et al. A soluble phosphorylated tau signature links tau, amyloid and the evolution of stages of dominantly inherited Alzheimer's disease. *Nat Med.* 2020;26:398–407.
57. Suarez-Calvet M, Karikari TK, Ashton NJ, Lantero Rodriguez J, Mila-Aloma M, Gispert JD, et al. Novel tau biomarkers phosphorylated at T181, T217 or T231 rise in the initial stages of the preclinical Alzheimer's continuum when only subtle changes in Aβ pathology are detected. *EMBO Mol Med.* 2020;12:e12921.
58. Mielke MM, Frank RD, Dage JL, Jeromin A, Ashton NJ, Blennow K, et al. Comparison of plasma phosphorylated tau species with amyloid and tau positron emission tomography, neurodegeneration, vascular pathology, and cognitive outcomes. *JAMA Neurol.* 2021;78:1108–17.
59. Samuels ER, Szabadi E. Functional neuroanatomy of the noradrenergic locus coeruleus: its roles in the regulation of arousal and autonomic function part I: principles of functional organisation. *Curr Neuropharmacol.* 2008;6:235–53.
60. Schwarz LA, Luo L. Organization of the locus coeruleus-norepinephrine system. *Curr Biol.* 2015;25:R1051–R1056.
61. Poe GR, Foote S, Eschenko O, Johansen JP, Bouret S, Aston-Jones G, et al. Locus coeruleus: a new look at the blue spot. *Nat Rev Neurosci.* 2020;21:644–59.
62. Schwarz LA, Luo L. Organization of the locus coeruleus-norepinephrine system. *Curr Biol.* 2015;25:R1051–1056.
63. Chan-Palay V, Asan E. Quantitation of catecholamine neurons in the locus coeruleus in human brains of normal young and older adults and in depression. *J Comp Neurol.* 1989;287:357–72.
64. Loughlin SE, Foote SL, Bloom FE. Efferent projections of nucleus locus coeruleus: topographic organization of cells of origin demonstrated by three-dimensional reconstruction. *Neuroscience.* 1986;18:291–306.
65. McKinney A, Hu M, Hoskins A, Mohammadyar A, Naeem N, Jing J, et al. Cellular and circuit organization of the locus coeruleus of adult mice. *BioRxiv.* 2022. <https://doi.org/10.1101/2022.03.01.481656>
66. Chandler DJ, Gao WJ, Waterhouse BD. Heterogeneous organization of the locus coeruleus projections to prefrontal and motor cortices. *Proc Natl Acad Sci USA.* 2014;111:6816–21.
67. Aston-Jones G, Waterhouse B. Locus coeruleus: from global projection system to adaptive regulation of behavior. *Brain Res.* 2016;1645:75–78.
68. Meyer PF, Ashton NJ, Karikari TK, Strikwerda-Brown C, Kobe T, Gonneaud J, et al. Plasma p-tau231, p-tau181, PET Biomarkers, and Cognitive Change in Older Adults. *Ann Neurol.* 2022;91:548–60.
69. Duyckaerts C, Braak H, Brion JP, Buee L, Del Tredici K, Goedert M, et al. PART is part of Alzheimer disease. *Acta Neuropathol.* 2015;129:749–56.
70. Fernandes P, Regala J, Correia F, Goncalves-Ferreira AJ. The human locus coeruleus 3-D stereotactic anatomy. *Surg Radio Anat.* 2012;34:879–85.

ACKNOWLEDGEMENTS

We would like to thank Dr. Gérard Bischof (University Hospital Cologne, Germany) for sharing the sliding window analyses code. This research was supported by Alzheimer Nederland major award WE.03–2019–02 (PI Heidi Jacobs, PhD), NIH grant

R01AG062559, R01AG068062 and R21AG074220 (PI Heidi Jacobs, PhD), P30AG1016, R01AG15819, R01AG17917 (PI, David Bennett, MD), and the BrightFocus Foundation A20211016F (PI: Maxime Van Egroo, PhD). OH is supported by the Swedish Research Council (2016–00906), the Knut and Alice Wallenberg foundation (2017–0383), the Marianne and Marcus Wallenberg foundation (2015.0125), the Strategic Research Area MultiPark (Multidisciplinary Research in Parkinson's disease) at Lund University, the Swedish Alzheimer Foundation (AF-939932), the Swedish Brain Foundation (FO2021–0293), The Parkinson foundation of Sweden (1280/20), the Cure Alzheimer's fund, the Konung Gustaf V:s och Drottning Victorias Frimurarestiftelse, the Skåne University Hospital Foundation (2020-O000028), Regionalt Forskningsstöd (2020–0314) and the Swedish federal government under the ALF agreement (2018-Projekt0279). HZ is a Wallenberg Scholar supported by grants from the Swedish Research Council (#2018–02532), the European Research Council (#681712 and #101053962), Swedish State Support for Clinical Research (#ALFGBG-71320), the Alzheimer Drug Discovery Foundation (ADDF), USA (#201809–2016862), the AD Strategic Fund and the Alzheimer's Association (#ADSF-21–831376-C, #ADSF-21–831381-C, and #ADSF-21–831377-C), the Bluefield Project, the Olav Thon Foundation, the Erling-Persson Family Foundation, Stiftelsen för Gamla Tjänarinnor, Hjärtfonden, Sweden (#FO2022–0270), the European Union's Horizon 2020 research and innovation programme under the Marie Skłodowska-Curie grant agreement No 860197 (MIRIADE), the European Union Joint Programme – Neurodegenerative Disease Research (JPN2021–00694), and the UK Dementia Research Institute at UCL (UKDRI-1003). KB is supported by the Swedish Research Council (#2017–00915), the Alzheimer Drug Discovery Foundation (ADDF), USA (#RDAPB-201809–2016615), the Swedish Alzheimer Foundation (#AF-930351, #AF-939721 and #AF-968270), Hjärtfonden, Sweden (#FO2017–0243 and #ALZ2022–0006), the Swedish state under the agreement between the Swedish government and the County Councils, the ALF-agreement (#ALFGBG-715986 and #ALFGBG-965240), the European Union Joint Programme for Neurodegenerative Disorders (JPN2019–466–236), the National Institute of Health (NIH), USA, (grant #1R01AG068398–01), and the Alzheimer's Association 2021 Zenith Award (ZEN-21–848495). H-SY is supported by NIH grant K23AG062750.

AUTHOR CONTRIBUTIONS

MVE analyzed the data, performed statistical analyses and wrote the manuscript. JMR aided in data collection of the 7T dataset, data interpretation, manuscript interpretation and writing of the manuscript. NJA, SJ, H-SY, KB, OH and HZ analyzed the blood samples, aided in interpretation of the results and manuscript preparation. RAS and KAJ provided conceptual advice, aided in interpretation of the results and manuscript preparation. DAB collected the ROSMAP data, aided in interpretation of the data and results, and manuscript preparation. HILJ designed the study, analyzed the data, performed statistical analyses, wrote the manuscript, supervised the project and provided funding. All authors discussed the results and implications and commented on various versions of the manuscript.

COMPETING INTERESTS

KAJ has served as paid consultant for Janssen, Novartis, Biogen, Roche, Lundberg, and Abbvie. He is a site co-investigator for Lilly/Avid and receives research support for clinical trials from Eisai, Lilly, and Cerveau. RAS has served as a paid consultant for Ionis, Shionogi, Biogen, Genentech, Oligomerix, Cytox, Acumen, JOMDD, Renew, Neuraly, AC Immune, Alnylam, Janssen, Neurocentria, Prothena, Eisai, Takeda and Roche and receives research support for clinical trials from Eisai, Eli Lilly, NIA and Alzheimer's Association. NJA has given lectures in symposia sponsored by Eli Lilly. OH has acquired research support (for the institution) from ADx, AVID Radiopharmaceuticals, Biogen, Eli Lilly, Eisai, Fujirebio, GE Healthcare, Pfizer, and Roche. In the past 2 years, he has received consultancy/speaker fees from AC Immune, Amylyx, Alzpath, BioArctic, Biogen, Cerveau, Fujirebio, Genentech, Novartis, Roche, and Siemens. HZ has served at scientific advisory boards and/or as a consultant for Abbvie, Acumen, Alector, ALZPath, Annexon, Apellis, Artery Therapeutics, AZTherapies, CogRx, Denali, Eisai, Nervgen, Novo Nordisk, Passage Bio, Pinteon Therapeutics, Red Abbey Labs, reMYND, Roche, Samumed, Siemens Healthineers, Triplet Therapeutics, and Wave, has given lectures in symposia sponsored by Cellectricon, Fujirebio, Alzecure, Biogen, and Roche, and is a co-founder of Brain Biomarker Solutions in Gothenburg AB (BBS), which is a part of the GU Ventures Incubator Program. KB has served as a consultant, at advisory boards, or at data monitoring committees for Abcam, Axon, BioArctic, Biogen, JOMDD/Shimadzu, Julius Clinical, Lilly, MagQc, Novartis, Ono Pharma, Pharmatrophix, Prothena, Roche Diagnostics, and Siemens Healthineers, and is a co-founder of Brain Biomarker Solutions in Gothenburg AB (BBS), which is a part of the GU Ventures Incubator Program. H-SY has received personal fees (honorarium) from Genentech,

Inc outside the submitted work. These relationships are not related to the content in the manuscript. All other authors report no relevant conflicts.

ADDITIONAL INFORMATION

Supplementary information The online version contains supplementary material available at <https://doi.org/10.1038/s41380-023-02041-y>.

Correspondence and requests for materials should be addressed to Heidi I. L. Jacobs.

Reprints and permission information is available at <http://www.nature.com/reprints>

Publisher's note Springer Nature remains neutral with regard to jurisdictional claims in published maps and institutional affiliations.



Open Access This article is licensed under a Creative Commons Attribution 4.0 International License, which permits use, sharing, adaptation, distribution and reproduction in any medium or format, as long as you give appropriate credit to the original author(s) and the source, provide a link to the Creative Commons license, and indicate if changes were made. The images or other third party material in this article are included in the article's Creative Commons license, unless indicated otherwise in a credit line to the material. If material is not included in the article's Creative Commons license and your intended use is not permitted by statutory regulation or exceeds the permitted use, you will need to obtain permission directly from the copyright holder. To view a copy of this license, visit <http://creativecommons.org/licenses/by/4.0/>.

© The Author(s) 2023